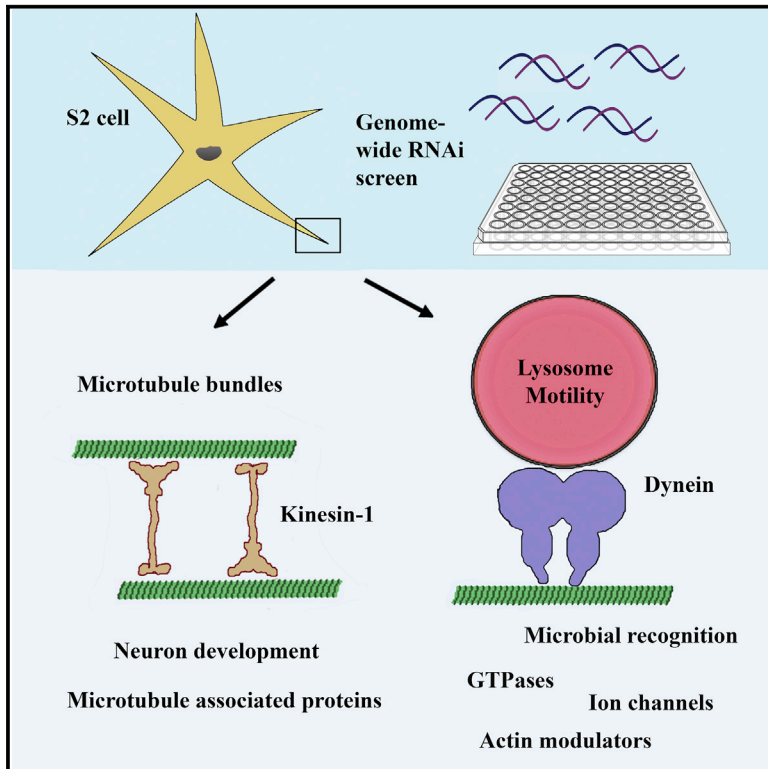


Cell Reports

A Genome-wide RNAi Screen for Microtubule Bundle Formation and Lysosome Motility Regulation in *Drosophila* S2 Cells

Graphical Abstract



Authors

Amber L. Jolly, Chi-Hao Luan, Brendon E. Dusel, ..., Deborah Dean, Andrew R. Cohen, Vladimir I. Gelfand

Correspondence

acohen@coe.drexel.edu (A.R.C.),
vgelfand@northwestern.edu (V.I.G.)

In Brief

Jolly et al. perform a genome-wide RNAi screen for factors involved in lysosome motility regulation. Actin is fragmented in S2 cells to allow for the formation of microtubule bundles, and lysosomes tracked along the bundles. They find that dynein and Rab7a have opposing effects on lysosome motility.

Highlights

- 15,683 genes are targeted by RNAi and tested for lysosome motility
- Lysosome motility is tracked in S2 cells along microtubule bundles
- Dynein heavy and light chains are required for lysosome motility
- Constitutively active Rab7a slows lysosome motility



A Genome-wide RNAi Screen for Microtubule Bundle Formation and Lysosome Motility Regulation in *Drosophila* S2 Cells

Amber L. Jolly,^{1,3} Chi-Hao Luan,² Brendon E. Dusel,² Sara F. Dunne,² Michael Winding,¹ Vishrut J. Dixit,¹ Chloe Robins,² Jennifer L. Saluk,² David J. Logan,⁴ Anne E. Carpenter,⁴ Manu Sharma,³ Deborah Dean,³ Andrew R. Cohen,^{5,*} and Vladimir I. Gelfand^{1,*}

¹Department of Cell and Molecular Biology, Northwestern University, Chicago, IL 60611, USA

²High Throughput Analysis Laboratory, Northwestern University, Evanston, IL 60208, USA

³Children's Hospital Oakland Research Institute, Oakland, CA 94609, USA

⁴Imaging Platform, Broad Institute of Harvard and MIT, Cambridge, MA 02142, USA

⁵Department of Electrical and Computer Engineering, Drexel University, Philadelphia, PA 19104, USA

*Correspondence: acohen@coe.drexel.edu (A.R.C.), vgelfand@northwestern.edu (V.I.G.)

<http://dx.doi.org/10.1016/j.celrep.2015.12.051>

This is an open access article under the CC BY license (<http://creativecommons.org/licenses/by/4.0/>).

SUMMARY

Long-distance intracellular transport of organelles, mRNA, and proteins (“cargo”) occurs along the microtubule cytoskeleton by the action of kinesin and dynein motor proteins, but the vast network of factors involved in regulating intracellular cargo transport are still unknown. We capitalize on the *Drosophila melanogaster* S2 model cell system to monitor lysosome transport along microtubule bundles, which require enzymatically active kinesin-1 motor protein for their formation. We use an automated tracking program and a naive Bayesian classifier for the multivariate motility data to analyze 15,683 gene phenotypes and find 98 proteins involved in regulating lysosome motility along microtubules and 48 involved in the formation of microtubule filled processes in S2 cells. We identify innate immunity genes, ion channels, and signaling proteins having a role in lysosome motility regulation and find an unexpected relationship between the dynein motor, Rab7a, and lysosome motility regulation.

INTRODUCTION

Numerous signaling cascades, receptors, and adaptor proteins appear to be involved in dictating the specificity of molecular motor activation/inactivation; however, an insufficient number of proteins have been identified to account for the complex regulation of motor activity and cargo transport (Kashina and Rodionov, 2005). Some of the accessory proteins have been identified in genetic screens and mutations in their genes are known causes of several neurodegenerative diseases such as lissencephaly (Vallee et al., 2001), Huntington's disease (Colin et al., 2008), and motor neuron disease (Chevalier-Larsen and Holzbaur, 2006). Unfortunately, genetic screens in multi-cellular or-

ganisms are difficult to perform and phenotypes related to mutations in motility-related genes are variable, making identification of interesting candidates problematic.

Bioinformatic techniques allowed for the identification of the motors themselves, because the ATPase motor domains are highly conserved. However, the majority of proteins involved in regulating cargo transport are not motors; instead, they might indirectly affect motor activity via a post-translational modification or by acting as a part of a tethering complex linking the motor with its cargo. It is well documented that multiple organelles are transported by the same motor, suggesting that motor type alone is not sufficient to dictate the specificity of organelle transport regulation. For example, conventional kinesin (kinesin-1) is known to move dFMR, an mRNA-protein complex (Ling et al., 2004), Merlin, a neurofibromatosis type 2 (NF2) tumor suppressor (Benseñor et al., 2010), and mitochondria (Pilling et al., 2006), among other cargoes. While kinesin-1 binds Merlin via its light chain, it does not require the light chain to bind dFMR (Ling et al., 2004) or mitochondria (Benseñor et al., 2010); instead, it uses the adaptor protein Milton to bind a mitochondrial GTPase Miro (Glater et al., 2006). Such motility proteins are not identifiable using bioinformatics approaches because of their structural and sequence heterogeneity. Uncharacterized motility factors are likely to elude most protein-protein interaction assays as well, because of their large size and/or transient nature of these protein complexes.

Designing a genomic screen for organelle motility is complicated because transport occurs along both actin and microtubule networks that overlap and are not perfectly spatially organized, making the cytoskeletal track and direction of transport questionable in most cultured cell systems. Furthermore, typical organelle motility regulation occurs at the level of individual organelles in tissue culture cells. Individual organelles undergo stochastic motility, stalling between runs to the plus and minus ends of polarized cytoskeletal elements, independent of other organelles. This makes it difficult to identify components involved in motility regulation using biochemical or microscopic methods, and model systems in which an entire organelle

population is simultaneously and homogeneously regulated are rare; the *Xenopus laevis* melanophore pigment cell is thus far the major system in which organelle transport regulation has been studied, taking advantage of the ability to induce the entire population of melanocytes to aggregate or disperse pigment granules (Nascimento et al., 2003).

To address these issues, we performed a genome-wide RNAi screen for intracellular transport regulation, tracking lysosome motility in the *Drosophila* S2 cell model system. S2 cells are widely used for RNAi-based experiments because of the highly efficient RNAi in these cells after incubation with long double-stranded RNAs (dsRNAs) even in the absence of a transfection step (Worby and Dixon, 2004). We developed our system to study microtubule based organelle transport separately from the transport of organelles along actin filaments by the action of myosin motors. Transport along these two cytoskeletal filaments is not typically separated, and organelles are able to switch their motility from one track to another (Slepchenko et al., 2007; Ali et al., 2007, 2008; Hendricks et al., 2010; Schroeder et al., 2010). We exposed S2 cells to the actin-fragmenting drug cytochalasin D while the cells are in suspension and subsequently plated on a concanavalin-A-coated surface. This causes them to form long unbranched processes filled with parallel microtubule bundles with the plus ends pointing toward the periphery (Kural et al., 2005). Since *Drosophila* cells do not contain cytoplasmic intermediate filaments (Goldstein and Gunawardena, 2000), they are optimal for organelle tracking as it is unperturbed by cell movements or actin dynamics or by the overlapping regions of the microtubule cytoskeleton with the actin or intermediate filament networks.

Cargo motility is highly sensitive to cytoplasmic ATP concentration, since motor proteins use ATP hydrolysis to power cargo transport. Any gene regulating the ATP concentration can impact lysosome motility. To overcome this, we analyzed lysosome motility only in cells having processes of a normal length, since the kinesin motor protein must function normally in order to form cellular processes. We previously published that the heavy chain of the conventional kinesin motor protein (KHC) utilizes a C-terminal microtubule-binding site to slide microtubules against one another and drive process formation (Jolly et al., 2010). We used this cell system in the current study to perform two screens: one for factors involved in regulating lysosome motility and the other for factors involved in process formation. Importantly, we used the measurements of process length to help identify factors involved in lysosome motility.

RESULTS

Screen for Organelle Transport Regulation in Living Cells

Genome-wide screening was performed to identify genes involved in regulating lysosome motility along microtubules in *Drosophila* S2 cells. For the primary and secondary screens, a library of long (200- to 800-bp) dsRNAs targeting confirmed and predicted coding sequences was purchased from Open Biosystems (Goshima et al., 2007). This library was created against 15,683 genes covering the entire predicted genome. The open reading frames covered include the initial genome identified in

the Berkeley *Drosophila* Genome Project (BDGP) and are identified by CG numbers and additionally include the predicted, but not yet validated, genes identified using the Heidelberg prediction (denoted by the hdc numbering system) (Hild et al., 2003).

We developed a 96-well plate automated live-cell assay employing fluorescence microscopy to follow lysosome motility along microtubule filled processes induced by culturing S2 cells in cytochalasin D. Treating S2 cells in this way causes the actin network to fragment, leaving only the microtubule cytoskeleton intact. Following RNAi, S2 cells were robotically plated onto concanavalin-A-coated glass bottom 96 well plates in media containing 5 μ M cytochalasin D for 3 hr to allow process growth and adhesion to the surface for improved microscopy. To stain the nucleus, lysosomes, and microtubules, Hoechst, Lyso-Tracker, and Tubulin Tracker dyes were added to cells and imaged using an ArrayScanVTI automated imager (Figure 1A). Figure 1B shows the workflow of the assay, and our predicted model for how the kinesin and dynein motor proteins contribute to the formation of the microtubule filled processes in S2 cells treated in this way.

In-house in-vitro-transcribed dsRNA against DHC was used to confirm knockdown of the protein to at least 80% of wild-type levels in the screen (Figure 2A). DHC was used in each plate as a motility and process formation control; we report here that it is involved in both phenotypes. An analysis of the cell morphology in the DHC controls revealed 2-fold longer processes found in the DHC controls as compared to mock treated cells (Figure 2B). Mock treated (wild-type) cells were included in each plate as negative controls (see Experimental Procedures).

Two types of image analyses were performed independently on the image sets to separately analyze process area and lysosome motility, and these parameters were compared post hoc. To identify genes involved in process formation, the nuclear and microtubule image sets were analyzed using CellProfile software (Carpenter et al., 2006). First, linear regions of interest were identified (the microtubule-filled processes), and each of these identified objects was skeletonized so that the length, but not the width, was analyzed (Figure 3A). The process area per cell was defined as the sum of the process lengths per image divided by the number of cells per image. Images from three fields in different locations within each well were analyzed independently, and the image with the maximal process area was used. This approach was taken to prevent data skewing due to out of focus images or local inconsistencies in cell density, which may affect the calculated process length, for example, because of processes overlapping cell bodies. This resulted in a single value representing the average process area per cell. The process formation hits identified in the primary genomic screen were validated in a separate secondary screen using the same dsRNA target sequences. The lysosome motility analysis was independently repeated with greater stringency and using new dsRNA sequences to eliminate off target effects.

KHC and DHC as Process Formation Controls

Our previous work revealed that following KHC RNAi, S2 cells lack the long neurite-like processes observed in wild-type cells (Jolly et al., 2010). The kinesin requirement can be attributed to the ability of KHC to slide microtubules against each other and

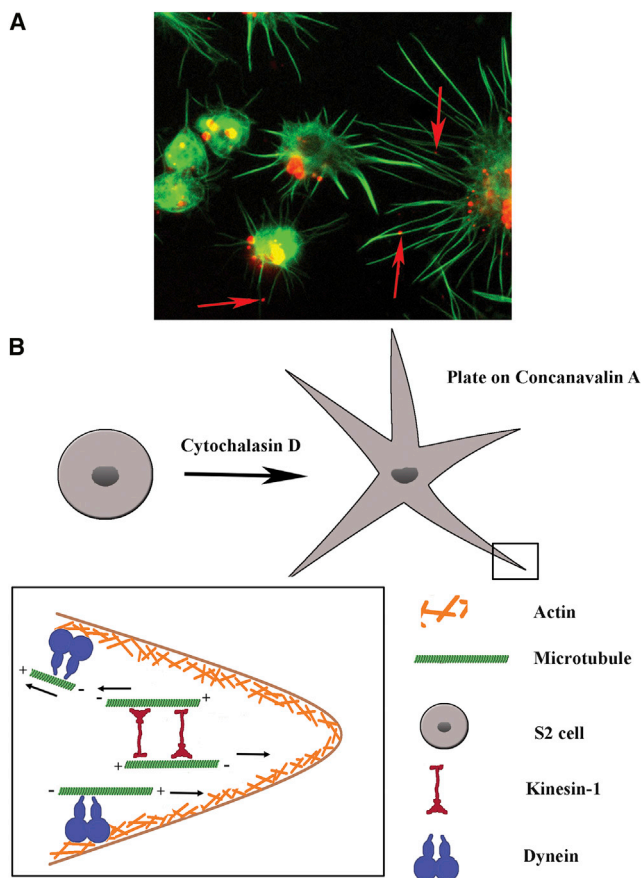


Figure 1. Image-Based Screen for Process Formation and Lysosome Motility along Microtubules in S2 Cells

(A) Overlay of the tubulin (Tubulin Tracker dye; green) and lysosome images (LysoTracker red dye, red) captured using the ArrayScanVTI automated imager. Lysosomes moving along microtubule bundles within the processes (indicated by the arrows) were followed for tracking, while the majority of the lysosome population in the cell body was not included in this study.

(B) Illustration of the screening approach. S2 cells are suspension cells, but when plated in the presence of cytochalasin D onto a concanavalin-A-coated surface, S2 cells form astral projections (processes) filled with microtubule bundles. Data show kinesin-1 motor protein contributes to the formation of these processes by sliding antiparallel microtubules against each other to drive process formation; data suggest dynein plays a role in microtubule organization, removing microtubules with plus ends pointing toward the nucleus from the processes.

drive process formation (Jolly et al., 2010). The computational method for process identification was designed using the KHC RNAi cell images as a control (Figure 3B). Therefore, cell projections with a width in the range of the large, wide cell bodies found in KHC knockdown cells were not considered valid processes and were eliminated from the analysis. We also included DHC RNAi as a second process formation control (Figure 3B).

Factors Involved in Process Formation

The average process length per cell was calculated for each well in the genomic screen and normalized to the mean of the entire genome (Figure 4A). The distribution of process area was unim-

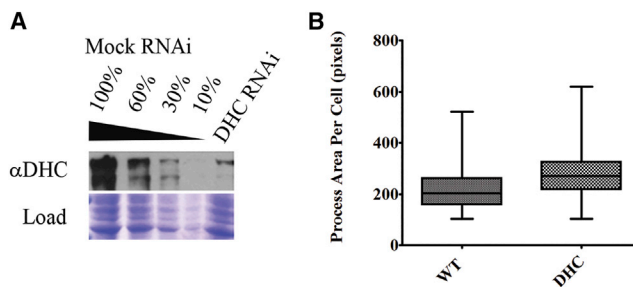


Figure 2. Dynein Heavy Chain as a Control in the Process Formation Screen

(A) Knockdown efficiency in 96-well plate format for the screening protocol determined using in-house in-vitro-transcribed DHC dsRNA. Top panel shows immunoblot against the dynein heavy chain, with dilutions of mock RNAi cells provided for an estimate of knockdown efficiency. Coomassie stain (bottom panel) was used as a loading control.

(B) Box plots of process formation in wild-type (mock) and DHC RNAi wells ($n = 140$ per condition) determined using the CellProfiler. The median process area per cell is 1.34-fold greater in DHC RNAi than in wild-type cells (271 versus 203, $p < 0.0001$, Mann-Whitney).

odal with a small right-handed tail. To establish thresholds for hit identification, length data from the genomic screen were compared to the mock-treated and DHC control wells included in each screen plate and to test plates containing half mock-treated and half KHC RNAi-treated wells. The strictly standardized mean difference (SSMD) compares the means and variances of the KHC and DHC RNAi average process length distributions and was 1.25, indicating a “moderate positive effect” (Zhang, 2007). We chose primary screen hits that were shorter than all those in the KHC distribution or longer than all those in the wild-type (mock) distribution. This was done to minimize the number of short process hits, which were overrepresented in the distribution, and maximize the number of long process hits, which were underrepresented. Using the distribution of mock-treated and KHC RNAi wells ($n = 142$ wells per condition), normalized to the mean of the genomic screen, we used a Z score of -2.2 to identify short process hits and a Z score of 3.7 to identify long process hits. At this level of stringency, 594 hits were selected for secondary screening (Figure 4B).

The secondary screen was performed by re-screening with the same dsRNA sequences in 96-well plate format, with mock-treated cells in half of each plate, and the average process length per cell was normalized to the mean of these mock-treated wells. A plot of the natural log distribution of the normalized mock treated wells is shown in Figure 4C, with vertical lines indicating the thresholds used to identify hits. The thresholds in the secondary screen were significant at a p value of less than 0.05. For the long process hits, this corresponds to the process length being at least twice the average wild-type length; for the short process hits, this corresponds to the process length being less than half the average wild-type length (Figure 4C). At this stringency, we expect 5% of the hits to be false positives; we therefore further filtered by eye in order to remove false positives including out of focus images and images having dead, floating, or missing cells. Of the 594 hits from the primary screen, 65 were validated in the secondary screen. This resulted in 31 hits having

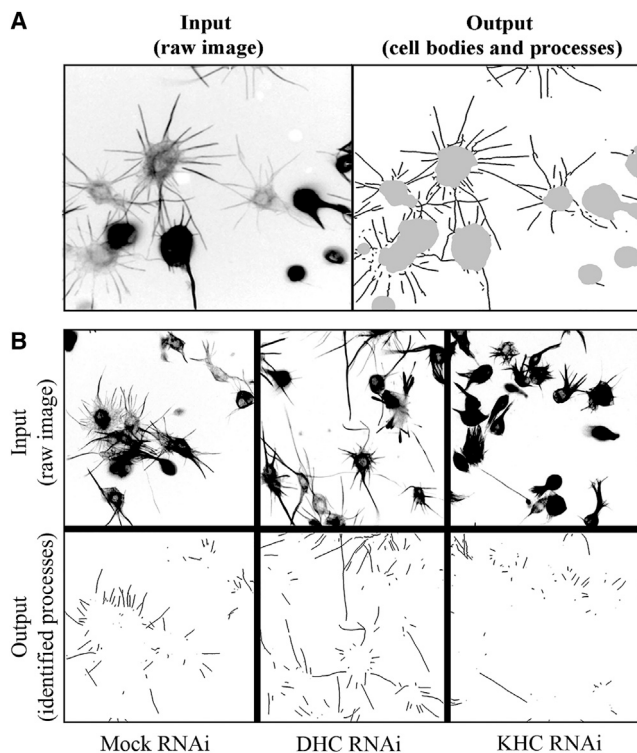


Figure 3. Image Analysis of S2 Cell Processes

(A) Analysis of a raw input image (left) to calculate the sum of the process lengths per cell body using CellProfiler (right). The nuclear (Hoechst) and microtubule images were used to identify the outlines of each cell body. Cell bodies were masked and only included processes are shown in the output images. Black lines denote process length calculation (width of every line set to one pixel), and cell bodies are indicated in gray. The total area covered by processes divided by the cell body count average was used to measure the average process length per cell.

(B) DHC and KHC as process formation screen controls. Images captured with the ArrayScanVTI instrument (top) were analyzed using CellProfiler (bottom).

significantly shorter processes than wild-type cells and 17 hits having significantly longer processes (Table S1).

Lysosome Motility Controls

In addition to identifying genes involved in the kinesin-dependent formation of cellular processes, we screened for genes involved in the regulation of lysosome motility along microtubules. While the motors that move lysosomes in *Drosophila* cells are unknown, cytoplasmic dynein has been implicated in lysosome motility in mice (Harada et al., 1998). In addition, both kinesin-1 and kinesin-2 have been implicated in lysosome motility in mammalian cells (Brown et al., 2005; Nakata and Hirokawa, 1995), but these studies suggest that neither motor alone is sufficient for plus-end-directed motility. Therefore, we set out to identify the *Drosophila* lysosomal motors using RNAi of cytoplasmic dynein, conventional kinesin, and kinesin 2 in our S2 cells.

Knockdown of the dynein heavy chain (DHC) prevented lysosomes from entering S2 cell processes; a handful of lysosomes that did enter the processes displayed impaired bidirectional

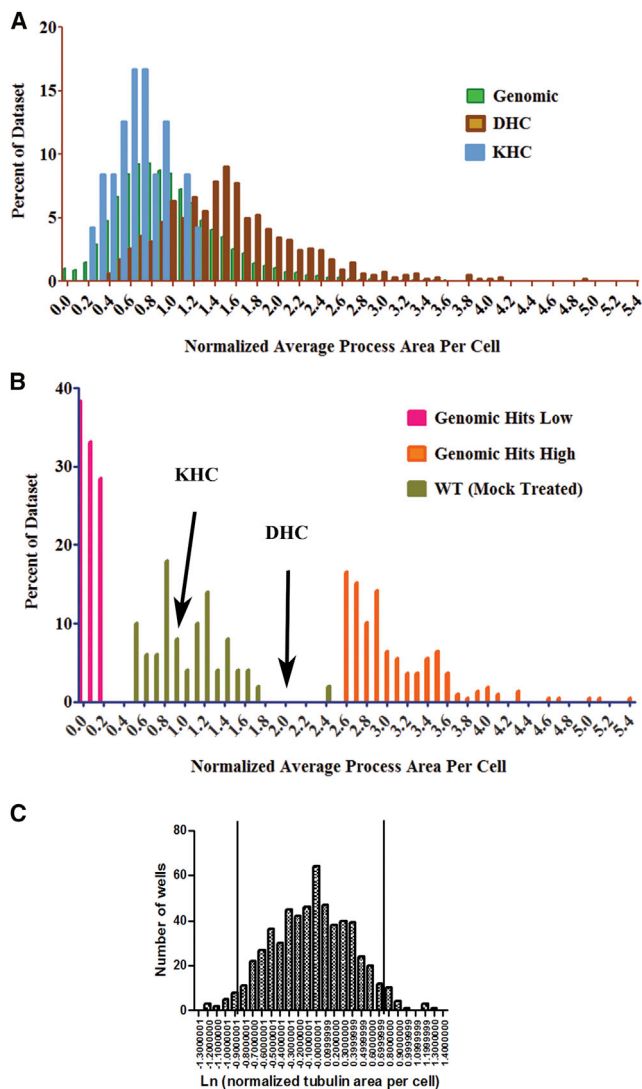


Figure 4. Threshold Criteria for the Process Area

(A) The per cell process area distributions of KHC and DHC RNAi control well images used to determine thresholds for hit identification in the genomic data. (B) High (long and/or numerous processes) and low (short and/or few processes) hits were identified in the primary screen using a highly conservative threshold such that the hits were found outside the distribution of mock-treated cells and also were above the mean DHC control well area or below the mean KHC control well area (arrows indicate the KHC and DHC well data found in the genomic screen and not the control wells).

(C) The thresholds for the second round of screening were determined using the distribution of mock treated cells included in the second round and setting $p < 0.05$. This corresponds to the process area being at least twice the area of the average wild-type for long process hits and less than half the average wild-type area for short process hits.

motility (the low level of motility is perhaps due to incomplete knockdown) (Figure 5). We hypothesized that knockdown of a minus-end motor would lead to the dispersion of lysosomes in the tips of the processes (the microtubule plus ends). Alternatively, the DHC RNAi is expected to completely block lysosome motility, but the distribution of lysosomes would be the same as

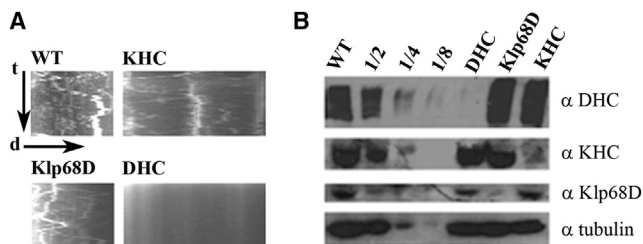


Figure 5. The Effect of Motor RNAi on Lysosome Motility in S2 Cells

(A) Kymographs of lysosome motility in a representative cytochalasin-D-induced process from cells following RNAi against dynein heavy chain (DHC), kinesin heavy chain (KHC), and kinesin-2 subunit Klp68D in *Drosophila* S2 cells stably expressing GFP-LAMP1. Length of each microtubule-filled process (d) is reflected in the length of each kymograph (cell body on the left and the peripheral tip of each process on the right). Time elapsed (t) is reflected in the y axis, and speed is indicated by the slope. Fluorescence time-lapse images acquired every 2 s for 2 min. WT, wild-type.

(B) Western blotting verifying successful RNAi. A dilution series of control (WT) cells was included to estimate the knockdown efficiency.

mock treated, as is the case for peroxisomes following DHC RNAi (Ling et al., 2004; Kim et al., 2007). The observed clustering of lysosomes near the cell body following DHC RNAi may therefore be more complicated, perhaps due to the overlapping roles of DHC in regulating both microtubule bundle/cell process formation and lysosome motility along the microtubule bundles. Even more surprising, neither kinesin-1 nor kinesin-2 RNAi had any apparent effect on lysosome motility (Figure 5).

Lysosome Motility Image Processing and Tracking Analysis

Candidate proteins involved in lysosome motility regulation were identified using image processing steps including image denoising and segmentation to identify moving lysosomes (Figures 6A–6D; Experimental Procedures). The results of the segmentation were input into the tracking algorithm. Although more sophisticated tracking approaches such as our own multitemporal association tracking (Winter et al., 2012) generally achieve higher accuracy by solving the tracking simultaneously over multiple image frames, for the present application, there were too few image frames (e.g., ten in the primary screen) to reliably apply such approaches. Instead, we used the single-frame assignment tracking algorithm we developed previously for tracking endosomes in zebrafish retina (Clark et al., 2011). This approach helps measure active powered, directional motion (taking into account velocity and excursion distance) along microtubule bundles. Motor-driven lysosome transport is characteristically stochastic (the organelle taking long directional runs followed by stops and changes in direction), although a basal level of unregulated diffusive motion cannot be excluded. Diffusive motility, however, is common to all of the conditions tested, allowing us to eliminate the contribution of diffusion to the phenotypes observed.

Following tracking, the median velocity and the maximal excursion distance for each track were stored for each image sequence. Using these data, a two-dimensional feature vector from each track was used to create a statistical model to identify candidate genes with a higher or lower degree of motility as

compared to mock treated cells. To create the thresholds, the primary screen data containing 17,570 candidate genes was considered (including controls added to the screening plates), with two replicate image sequences captured per gene (~20 cells analyzed per silenced gene) for a total of 35,140 image sequences. Within the screening data, there were 768 controls known to be non-motile (DHC RNAi cells) and 56 manually identified high-motility controls. Figure 6E shows the probability distributions for these control data. Classifying each of the controls, using a maximum likelihood approach under both distributions and discarding control wells where the two replicate image sequences classified differently, resulted in a classification accuracy of 94%. The 95% confidence interval for this classification was [0.91, 0.95]. Each of the remaining conditions was classified against the cumulative distribution function (CDF) for the motile and non-motile control data. Those conditions falling in the 95% or higher range of the CDF were selected for subsequent re-screening.

The results of the primary genomic screen for lysosome motility were validated in a secondary and tertiary screen. The secondary screen was performed using the same dsRNA sequences as in the primary genome-wide screen. After the first screen there were fewer control conditions available, so a single distribution was used for classification (Figure 6F). Three replicates were used in the secondary screen (approximately 30 cells per silenced gene) and classified with the requirement that all three replicates must agree or that there was a very strong motion response—greater than 16th percentile or 1 SD below the mean. These hits were then visually inspected for validation, resulting in the identification of 203 non-motile hits and 108 highly motile hits to re-screen. To further narrow the list, genes involved in transcription, ribosomal constituents, cuticle proteins, and chitin metabolism were removed, giving a final list of 157 low-motility and 89 high-motility hits. Table S2 lists the genes identified in the primary and secondary screens but excluded from the tertiary screen. In the tertiary screen, we used a new set of dsRNA sequences from the Harvard *Drosophila* RNAi screening center. New dsRNAs, targeting distinct amplicons, were used to remove hits arising due to possible off-target effects of the RNAi. A 90% threshold on the CDF was used to determine enhanced and decreased motility. Of 246 genes screened (9 were not available in the Harvard database), we identified 88 non-motile hits and 10 highly motile hits (Table S3; Movies S1, S2, and S3).

Effect of Overexpression of Wild-Type, Dominant-Negative, and Constitutively Active Rab7a on Lysosome Motility

Published studies would lead us to hypothesize that Rab7 and DHC RNAi would both give the same phenotype; i.e., a loss in motility. These studies (Jordens et al., 2001; Johansson et al., 2007) suggest Rab7a acts as a tether to bind dynein to lysosomes via accessory proteins. Yet, in this study, Rab7a RNAi resulted in a high-motility phenotype with the greatest confidence. To investigate this further, S2 cells were transfected with wild-type, dominant-negative, or constitutively active forms of Rab7a and analyzed for the effect on lysosome motility. Consistent with this phenotype, we found that lysosomes in cells expressing dominant-negative Rab7a paused less frequently than in cells expressing wild-type Rab7a or dominant-negative

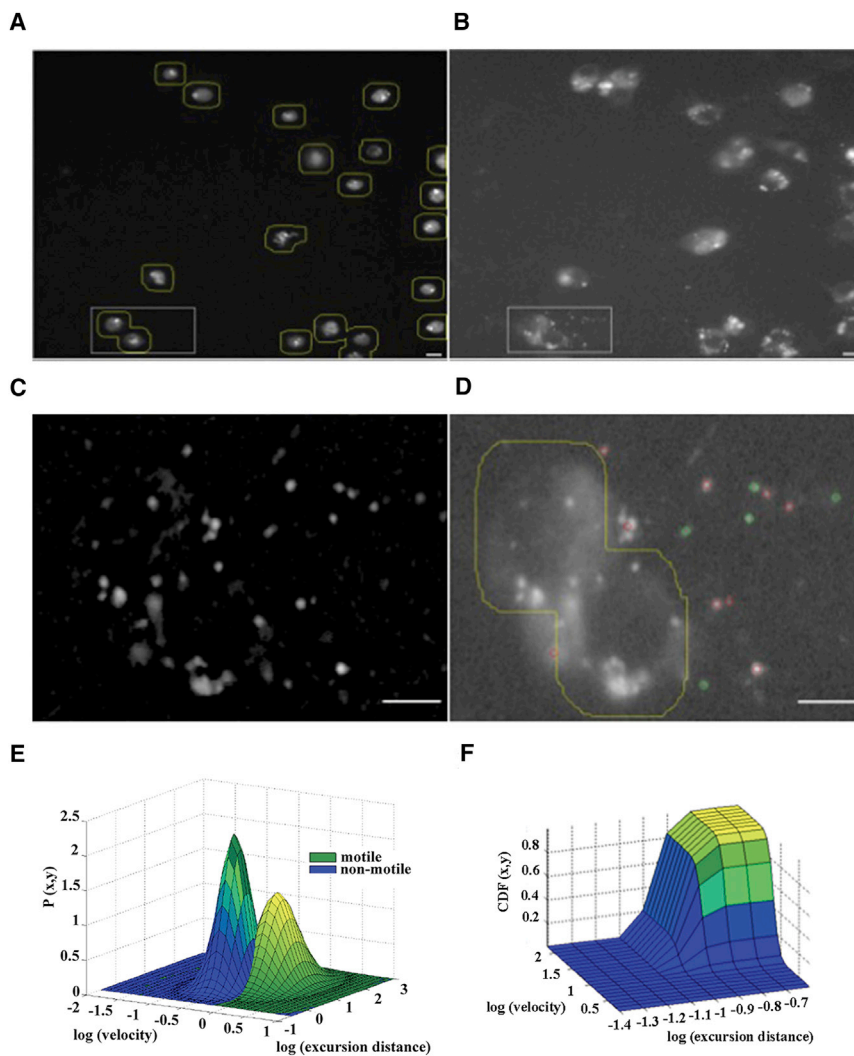


Figure 6. Image Processing Pipeline and Lysosome Tracking Analysis

(A–C) The nuclear (A) and lysosome (B) images were used for the lysosome tracking. Nuclear regions were segmented (yellow lines, A), and lysosomes within these regions excluded from further analysis. The lysosome channel image was denoised as in (C), zoomed to the rectangle shown in (A) and (B). Following denoising, organelles were identified.

(D) An example shows the original lysosome image with nuclear segmentation (yellow) and organelle segmentations circled in green and red. Only the organelles marked in red were successfully tracked through enough frames to contribute to classification. Scale bars, 5 μm .

(E) In the primary screen, probability density functions were estimated for motile and non-motile classes.

(F) In the secondary and tertiary screens, cumulative distribution functions were estimated for the wild-type (mock-treated) cells (shown here is the distribution for the secondary screen).

analysis. We anticipate that GFP tagging would allow researchers to use this system to track any cargo of choice. The obvious drawback to this system is the multiple functions performed by motor proteins, which makes the cellular phenotype more complicated. This is exemplified by the fact that KHC is involved in the formation and outgrowth of microtubule-based processes in addition to its role in regulating organelle motility along microtubules. Likewise, DHC is involved in microtubule bundle organization and length as well as organelle motility along these bundles. To differentiate between

Rab7a (Figure 7B). However, the dominant-negative Rab7a did not affect lysosome speed (Figure 7A) or pause duration (Figure 7C). Overexpression of a constitutively active form of Rab7a resulted in a loss in motility as compared to overexpression of the wild-type form of Rab7a. Specifically, constitutively active Rab7a resulted in a decreased speed (Figure 7A) and a longer pause time compared to wild-type Rab7a (Figure 7C).

DISCUSSION

We performed an automated live-cell genomic RNAi screen for organelle motility regulation. The methods used here are widely applicable to the study of cargo transport using the S2 cell model system. The advantages of the S2 system include the ability to study one cytoskeletal network in isolation; we analyzed motility along microtubules, but others could also study actin-based motility regulation after depolymerization of microtubules, for example. We used fluorescent dyes to label lysosomes rather than GFP-tagging lysosome-associated proteins to achieve homogenous and bright fluorescence levels critical to our image

these potentially overlapping phenotypes, each function was separately considered.

Remarkably, 15% of the final validated hits for process formation are well-characterized neuronal genes (Figure S1A). This represents more than the number of cytoskeletal hits or hits known to regulate microtubule dynamics. It is also approximately twice as many neuronal genes as would be expected from a random sampling of the genome (Figure S1B). Included in this list are neuronal genes not expected to play structural or cytoskeletal roles, such as CG2893, a calcium, potassium: sodium antiporter found in glial cells. This preponderance of “neuronal” genes may reflect a similarity in *Drosophila* S2 processes and neurites and suggests that the parallel microtubule bundles found in S2 processes and in axons are similar not just in the structural sense but in terms of regulation as well. This supports our finding that kinesin-mediated microtubule sliding drives early neurite formation and axon regeneration in primary *Drosophila* neurons (Lu et al., 2013, 2015).

In addition to neuronal genes, several genes involved in regulating microtubule dynamics were identified, including Klp10A.

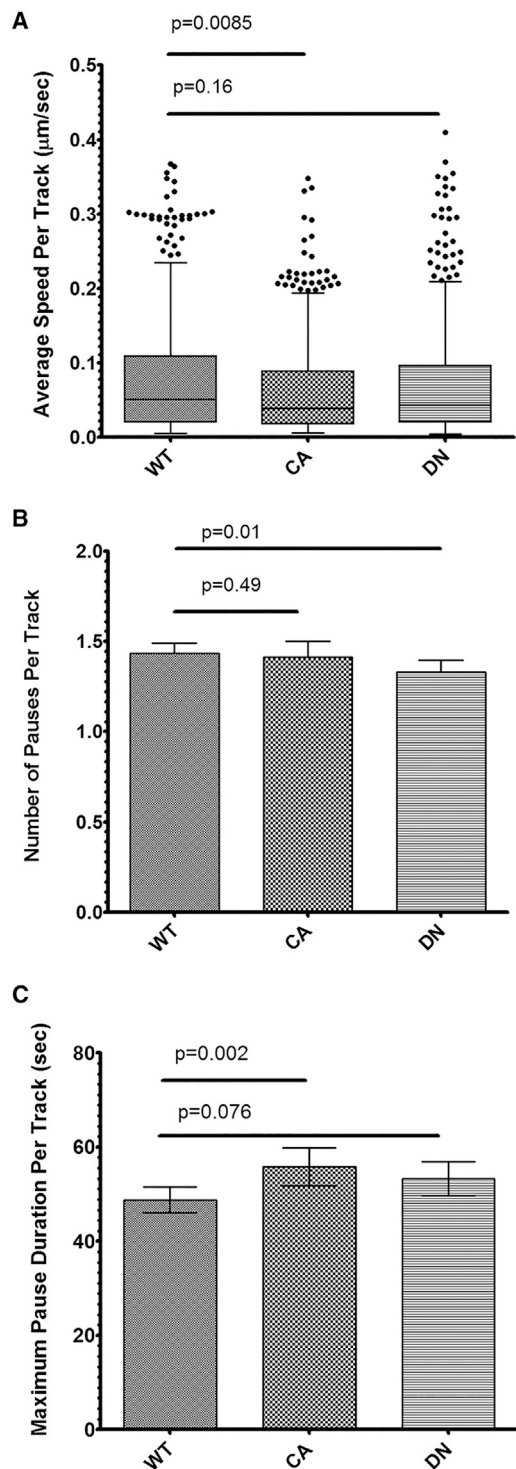


Figure 7. Effect of Constitutively Active and Dominant-Negative Rab7a on Lysosome Motility

S2 cells were transfected with plasmids encoding GFP-tagged wild-type (WT), constitutively active (CA), or dominant-negative (DN) forms of Rab7a, and the GFP-expressing organelles (lysosomes) from five movies per condition were tracked (each having approximately 10–20 cells). The average track speed measurements are displayed as box plots (A). Lysosomes were approximately four to five pixels in diameter; all lysosomes having a displacement of greater

As might be expected, RNAi of Klp10A leads to the formation of very long processes. This microtubule depolymerizing kinesin plays a role in depolymerizing microtubules in the mitotic spindle, along with another kinesin, Klp59C. However, during interphase, Klp10A is required to initiate microtubule depolymerization, while Klp59C continues to induce depolymerization following initiation (for review, see Sharp et al., 2005). This may explain why we did not identify Klp59C in our screen. Klp10A was the only motor protein identified as involved in process formation besides the control KHC and DHC motors. The hits also included Tao-1 kinase (CG14217), previously identified in the literature to induce process formation in S2 cells following RNAi even without the use of any chemical inhibitor to disrupt the actin network (Liu et al., 2010).

Encouragingly, of the factors identified in regulating lysosome motility, dynein light intermediate chain was identified as the non-motile hit with the greatest confidence (DHC was also present among the genome-wide set of dsRNAs screened and also identified as a non-motile hit, but it was excluded because of the long processes in DHC RNAi cells). Dynein light intermediate chain, along with dynein heavy chain, forms an essential part of the dynein motor protein complex. It is interesting that the other dynein subunits appear to be less penetrant in this screen. Many of dynein's accessory chains and subunits appear as hits in the primary screen (with the exception of ZW10, NUDEL, LIS1, and LC7, which all resulted in short processes and were excluded). However, these accessory proteins do not make it past the more stringent criteria in the secondary and tertiary screens. This may be related to a lack of RNAi efficiency due to protein stability. However, it is also likely that these subunits have differing effects on microtubules and/or motility (which appears to be true for ZW10, NUDEL, LIS1, and LC7).

Rab7a was also identified in lysosome motility regulation, although it was unexpectedly the high-motility hit with the greatest confidence. Rab7a is known to control the fusion of late endosomes with lysosomes (Bucci et al., 2000) and is thought to tether dynein to lysosomes. In mammalian cells, Rab7 has been implicated in recruiting the dynein/dynactin complex to lysosomes through Rab7-interacting lysosomal protein (RILP) and thereby inducing the aggregation of lysosomes around the perinuclear microtubule organizing center (MTOC) (Jordens et al., 2001). A follow-up study showed that Rab7 binds to the C-terminal 25 amino acids of p150^{Glued}, a component of the dynactin complex required for dynein activity (Johansson et al., 2007). Our data, on the other hand, show that Rab7a RNAi or expression of dominant-negative Rab7a both result in a high-motility phenotype, the opposite of what would be expected if Rab7a were a tether for the dynein motor protein. Likewise, expression of constitutively active Rab7 results in a decrease in both lysosome speed and time spent moving. This suggests that GTP-bound (active) Rab7a suppresses lysosome motility, and we may speculate this is related to its role in mediating organelle fusion, an event likely to slow organelle motility.

than one pixel (0.22 µm) between consecutive frames were considered moving and included in the analysis of pause number (B) and duration (C) (mean and 95% confidence intervals). The Mann-Whitney test was used to calculate p values.

In addition to Rab7a, the Rab-associated GDI interacting protein 3 and Rho GTPase activating protein at 54D were hits whose knockdown resulted in a non-motile phenotype. A putative Rho guanine nucleotide exchange factor, Cdep, was also identified. All these hits are likely to form a linker protein complex between the motor(s) that move lysosomes and the lysosomal membranes.

Strikingly, the screen did not identify any kinesin motor proteins responsible for transporting lysosomes toward the plus ends of microtubules. RNAi of CG3499, an unnamed protein containing an AAA+ ATPase domain, resulted in loss of lysosome motility and was identified as a high-confidence hit. The presence of the AAA+ domain makes this a candidate motor protein, although this is the protein fold used by the minus-end motor dynein and not by any known kinesin motor proteins. Another explanation is that plus-end movement of lysosomes is powered by multiple motors simultaneously. A well-documented example of multiple kinesins moving the same cargo is intraflagellar transport in *C. elegans*, where the same particle is transported by two members of the kinesin II family (Pan et al., 2006).

Two proteins involved in maintaining the actin filament network were identified as high-motility hits following knockdown: Arp2/3 and Actin 87E. These hits may have been identified due to incomplete F-actin depolymerization by our cytochalasin treatment or because of a novel role for these genes unrelated to their relationship with actin filaments. However, it is likely the former, since cytochalasin D treatment results in fragmentation of actin filaments rather than their complete depolymerization (Simpson and Spudich, 1980; Brenner and Korn, 1979). This finding is consistent with other studies indicating that the presence of actin can slow cargo transport along microtubules (Slepchenko et al., 2007; Ali et al., 2007, 2008; Hendricks et al., 2010; Schroeder et al., 2010).

Six of the non-motile hits (8%) are known to be involved in microbial recognition or to contain an immunoglobulin fold. This link between microbial detection systems and lysosome motility regulation remains to be explored, given the requirement for intracellular pathogens to avoid death in a lysosome via the phagocytic pathway. Additionally, several unexpected and interesting hits suggest crosstalk between ion channels, the innate immune system, the actin network, and microtubule-based lysosome motility. Further work will be required to place these components into their particular roles in the regulation of lysosome motility.

EXPERIMENTAL PROCEDURES

Primary and Secondary Screening Protocol Using the Open Biosystems dsRNA Library

For RNAi in a 96-well plate format, we used 1.3 μg dsRNA per well of a cone-bottom polypropylene plate and added 8×10^4 wild-type S2 cells ($100 \mu\text{l}$ of 8×10^5 cells/ml) in Insect Xpress media (Lonza) supplemented with 100 $\mu\text{g}/\text{ml}$ Primocin (Invivogen). Control DHC RNA was added to four wells per plate (created using an in vitro transcription reaction and purified using lithium chloride extraction). Plates were shaken at 300 rpm for 4 days to induce knockdown. The dsRNA library was purchased from Open Biosystems (catalog # RDM4412, lot #L001). Each well contained one dsRNA amplicon targeting exactly one open reading frame. At the time of plating, cytochalasin D was added to a final concentration of 5 μM and the cells were mixed. The cells were then placed on a flat surface to allow the growth of long microtubule-filled pro-

cesses. After 3 hr, a final concentration of 0.5 $\mu\text{g}/\text{ml}$ Hoechst dye and 25 nM LysoTracker red was added and the lysosome motility recorded (ten frames captured every 1 s per field). The ArrayScan automatically focused in the nuclear channel and captured all channels. After a further 2 hr (required to capture movies in two fields per well for a 96-well plate), 250 nM Oregon-green-labeled taxol was added, and after gentle shaking, the nuclei and microtubule networks were imaged using an automated ArrayScanVTI plate-reader from Cellomics. We captured lysosome movies in two different locations (fields) within each well and tubulin images in three different fields in order to verify the accuracy of each image and avoid imaging areas with sparse or dense cell growth or focus issues. The image analysis function of the plate reader was disabled, allowing us to simply acquire images with a dry 40 \times 0.75 numerical aperture objective, and take advantage of the automated focusing function.

Tertiary Screening Using Harvard dsRNA Sequences

The tertiary screen was performed on S2 cells constitutively expressing mCherry-tubulin. As before, except without robotics, cells were plated at 8×10^4 in each well of a 96-well plate and incubated with 1 μg dsRNA for 4 days prior to adding cytochalasin D and plating on concanavalin A before adding LysoTracker red. dsRNAs were purchased from the Harvard *Drosophila* RNAi Research Center. Images were captured on a Nikon TE-2000 microscope equipped with Yokogawa CSU-10 spinning disk, perfect focus, an encoded stage, and an Evolve 512 EMCCD camera.

Process Formation Screen Image Analysis

Image analysis was performed using CellProfiler (Carpenter et al., 2006) (<http://www.cellprofiler.org>). An image analysis pipeline was constructed to measure mCherry-labeled tubulin and Hoechst-stained nuclei. Each well's image set was analyzed independently, and the image processing was parallelized. The analyzed data were merged and stored in a MySQL (Oracle) database with subsequent analysis performed in Microsoft Excel.

Each field was processed in CellProfiler to identify nuclei and subsequently measure and identify tubulin-stained processes using the nuclei as seed objects. First, from the nuclear channel, presumed nuclei objects were enhanced and background reduced using a tophat filter with a structuring element of pixel size 40 (on the order of the nuclei size). A Gaussian filter (30 pixels wide) was used to further smooth the nuclei to reduce segmentation artifacts. Nuclei were segmented using a robust method thresholding pixels brighter than the mean intensity plus two times the SD, while first trimming the brightest and dimmest 5% of pixels. A filter step was included to exclude any spurious objects that were very eccentric (>0.95), i.e., not round. Then, cell bodies were detected from the tubulin channel by first suppressing small features, including thin dendritic processes, with a smoothing operation. The cell bodies were then thresholded in the tubulin channel using the nuclei objects as seed points via the thresholding method described above.

The tubulin containing processes were enhanced using a "tubeness" filter (Sato et al., 1998), which uses the eigenvalues of the Hessian matrix on the tubulin channel via an ImageJ bridge (Rasband, 1997–2011) to CellProfiler. Tubulin objects were then segmented from the tubeness-filtered images. Morphological operators were used on the tubulin objects to measure their overall length, including skeletonization (reducing the width down to a single pixel), de-spurring (removal of short branches), and cleaning (removal of isolated pixels). The morphological operators were calculated using MATLAB functions (MathWorks). Multiple measures including total length per field and number of branchpoints were recorded. The pipeline can be downloaded at http://cellprofiler.org/published_pipelines.shtml.

Lysosome Tracking Program

Figure 6 illustrates the image processing steps used to identify lysosomes. Following image processing, median track velocity and excursion distance were extracted for control and experimental data (these track features were used for all three motility screens). Excursion distance is measured as the maximum separation between any two points on the organelle track. The image denoising uses an approach proposed for protein image denoising (Michel et al., 2007) and subsequently applied by us for 2D organelle images (Chenouard et al., 2014) and 3D stem cell time-lapse images (Wait et al., 2014).

This approach models the noise as slow varying background combined with high-frequency shot noise. Each of these noise components is filtered separately. The slow varying background is filtered using a low-pass Gaussian filter. A median filter removes the high-frequency shot noise. Figure 6C shows an example denoised region of an organelle image. Following denoising, the images were segmented. A single nuclear channel image is segmented to estimate the nuclear location so organelles inside the nucleus can be excluded. The nuclear image is segmented using an adaptive threshold identified with the Otsu method (Otsu, 1979), combined with a small (three-pixel) morphological dilation operator. Sample nuclear channel segmentation results are shown in Figure 6A. The organelle segmentation uses the intensity values in the denoised image as input to a connected component analysis. The connected component analysis discards any potential organelles that are too large or too small or that fall outside a nuclear boundary. Figure 6D shows an example organelle segmentation result.

RNA Synthesis and Purification

dsRNA was transcribed in vitro with T7 polymerase and purified using LiCl extraction (Ally et al., 2009). Primers used in PCR reactions to create T7 templates from cDNA were as follows (T7 promoter sequences [5'-TAATAC GACTCACTATAGGG-3'] were added to the 5' end of each primer): KHC: forward, 5'-ATGTCCTCACACCAGAAGAAGC-3'; reverse, 5'-GGTGAGGAT GATGTTCTGAAGC; DHC: forward, 5'-AAACTCAACAGAATTAACGCC-3'; reverse, 5'-TTGGTACTGTGCACACCACT; Klp68D: forward, 5'-CATGAT CAAAATCGAGATGTGC-3'; reverse, 5'-AAGTTGACCCTCCAATTCTGC-3'.

Cloning of Rab7a Constructs

The *Drosophila melanogaster* full-length Rab7a coding sequence was inserted into pAc.A between Not1 and Xba1. The GFP coding sequence was N terminal, between Kpn1 and EcoRI. To create the dominant-negative and constitutively active Rab7a constructs, PCR was used to introduce mutations into the wild-type pAc-GFP-Rab7a plasmid, followed by ligation using the Phusion Site-Directed Mutagenesis kit (Thermo Scientific). The dominant-negative Rab7a (T22N) mutant was created using the following primers (5' phosphorylated): forward, 5'-AGCAGTGTGGGCAAGAAGTCTCTGTGAATCAG-3'; reverse, 5'-GTCGCCCAAGTATGACTTTTCAGTAGGGATTTCTTACGTC-3'. The constitutively active Rab7a (Q67L) mutant was created using the primers (5' phosphorylated): forward, 5'-TGGGACACTGCTGGTCTGGAACGCT TCCAGTCG-3'; reverse, 5'-GATCTGCATTGTGACCACTCGGGTGTGACCA CCA-3'.

Transfection and Tracking of S2 Cells Expressing Rab7a

S2 cells were transfected with Effectene transfection reagent (QIAGEN) according to the manufacturer's instructions. Images of GFP-Rab7a were acquired every 2 s for 2 min in the green channel and the movement of GFP-Rab7a-expressing lysosomes tracked using the Diatrack software. The maximum displacement was four pixels between consecutive frames. Identified tracks were then sorted according to a lifetime minimum of three frames and a length minimum of eight pixels. Gaps closure and track smoothing were performed.

SUPPLEMENTAL INFORMATION

Supplemental Information includes one figure, three tables, and three movies can be found with this article online at <http://dx.doi.org/10.1016/j.celrep.2015.12.051>.

AUTHOR CONTRIBUTIONS

Conceptualization and Methodology, V.I.G. and A.L.J.; Software, A.R.C., C.L., D.J.L., and A.E.C.; Investigation, A.L.J., B.E.D., S.F.D., M.J.W., V.J.D., C.R., and J.L.S.; Project Administration, A.L.J.; Writing, A.L.J.; Formal Analysis, Data Curation and Visualization, A.L.J., A.R.C., and M.S.; Resources, D.D.; Funding Acquisition, V.I.G., A.E.C., and C.L.; Supervision, V.I.G., A.R.C., and A.E.C.

ACKNOWLEDGMENTS

We would like to thank Pradeep Sivakumar (Northwestern University, Evanston, IL), Mark Bray, and the Carpenter lab (Broad Institute, MA) for help with batch image data processing. The project described was supported in part by the H Foundation Cancer Research Fund and Robert H. Lurie Comprehensive Cancer Center. The content is solely the responsibility of the authors and does not necessarily represent the official views of the H Foundation and Robert H. Lurie Comprehensive Cancer Center. Additional funding was provided by a National Science Foundation Graduate Research Fellowship Program fellowship to A.L.J. and National Institute of General Medical Science/National Institutes of Health grants R01 GM052111 to V.I.G. and R01 GM089652 to A.E.C.

Received: July 6, 2015

Revised: October 21, 2015

Accepted: December 7, 2015

Published: January 7, 2016

REFERENCES

- Ali, M.Y., Kremntsova, E.B., Kennedy, G.G., Mahaffy, R., Pollard, T.D., Trybus, K.M., and Warshaw, D.M. (2007). Myosin Va maneuvers through actin intersections and diffuses along microtubules. *Proc. Natl. Acad. Sci. USA* *104*, 4332–4336.
- Ali, M.Y., Lu, H., Bookwalter, C.S., Warshaw, D.M., and Trybus, K.M. (2008). Myosin V and Kinesin act as tethers to enhance each others' processivity. *Proc. Natl. Acad. Sci. USA* *105*, 4691–4696.
- Ally, S., Larson, A.G., Barlan, K., Rice, S.E., and Gelfand, V.I. (2009). Opposite-polarity motors activate one another to trigger cargo transport in live cells. *J. Cell Biol.* *187*, 1071–1082.
- Benseñor, L.B., Barlan, K., Rice, S.E., Fehon, R.G., and Gelfand, V.I. (2010). Microtubule-mediated transport of the tumor-suppressor protein Merlin and its mutants. *Proc. Natl. Acad. Sci. USA* *107*, 7311–7316.
- Brenner, S.L., and Korn, E.D. (1979). Substoichiometric concentrations of cytochalasin D inhibit actin polymerization. Additional evidence for an F-actin treadmill. *J. Biol. Chem.* *254*, 9982–9985.
- Brown, C.L., Maier, K.C., Stauber, T., Ginkel, L.M., Wordeman, L., Vemos, I., and Schroer, T.A. (2005). Kinesin-2 is a motor for late endosomes and lysosomes. *Traffic* *6*, 1114–1124.
- Bucci, C., Thomsen, P., Nicoziani, P., McCarthy, J., and van Deurs, B. (2000). Rab7: a key to lysosome biogenesis. *Mol. Biol. Cell* *11*, 467–480.
- Carpenter, A.E., Jones, T.R., Lamprecht, M.R., Clarke, C., Kang, I.H., Friman, O., Guertin, D.A., Chang, J.H., Lindquist, R.A., Moffat, J., et al. (2006). CellProfiler: image analysis software for identifying and quantifying cell phenotypes. *Genome Biol.* *7*, R100.
- Chenouard, N., Smal, I., de Chaumont, F., Maška, M., Sbalzarini, I.F., Gong, Y., Cardinale, J., Carthel, C., Coraluppi, S., Winter, M., et al. (2014). Objective comparison of particle tracking methods. *Nat. Methods* *11*, 281–289.
- Chevalier-Larsen, E., and Holzbaur, E.L. (2006). Axonal transport and neurodegenerative disease. *Biochim. Biophys. Acta* *1762*, 1094–1108.
- Clark, B.S., Winter, M., Cohen, A.R., and Link, B.A. (2011). Generation of Rab-based transgenic lines for in vivo studies of endosome biology in zebrafish. *Dev. Dyn.* *240*, 2452–2465.
- Colin, E., Zala, D., Liot, G., Rangone, H., Borrell-Pagès, M., Li, X.J., Saudou, F., and Humbert, S. (2008). Huntingtin phosphorylation acts as a molecular switch for anterograde/retrograde transport in neurons. *EMBO J.* *27*, 2124–2134.
- Glater, E.E., Megeath, L.J., Stowers, R.S., and Schwarz, T.L. (2006). Axonal transport of mitochondria requires mitorin to recruit kinesin heavy chain and is light chain independent. *J. Cell Biol.* *173*, 545–557.
- Goldstein, L.S., and Gunawardena, S. (2000). Flying through the *Drosophila* cytoskeletal genome. *J. Cell Biol.* *150*, F63–F68.

- Goshima, G., Wollman, R., Goodwin, S.S., Zhang, N., Scholey, J.M., Vale, R.D., and Stuurman, N. (2007). Genes required for mitotic spindle assembly in *Drosophila* S2 cells. *Science* *316*, 417–421.
- Harada, A., Takei, Y., Kanai, Y., Tanaka, Y., Nonaka, S., and Hirokawa, N. (1998). Golgi vesiculation and lysosome dispersion in cells lacking cytoplasmic dynein. *J. Cell Biol.* *141*, 51–59.
- Hendricks, A.G., Perlson, E., Ross, J.L., Schroeder, H.W., 3rd, Tokito, M., and Holzbaur, E.L. (2010). Motor coordination via a tug-of-war mechanism drives bidirectional vesicle transport. *Curr. Biol.* *20*, 697–702.
- Hild, M., Beckmann, B., Haas, S.A., Koch, B., Solovyev, V., Busold, C., Fellenberg, K., Boutros, M., Vingron, M., Sauer, F., et al. (2003). An integrated gene annotation and transcriptional profiling approach towards the full gene content of the *Drosophila* genome. *Genome Biol.* *5*, R3.
- Johansson, M., Rocha, N., Zwart, W., Jordens, I., Janssen, L., Kuijil, C., Olkkonen, V.M., and Neefjes, J. (2007). Activation of endosomal dynein motors by stepwise assembly of Rab7-RILP-p150Glued, ORP1L, and the receptor betall spectrin. *J. Cell Biol.* *176*, 459–471.
- Jolly, A.L., Kim, H., Srinivasan, D., Lakonishok, M., Larson, A.G., and Gelfand, V.I. (2010). Kinesin-1 heavy chain mediates microtubule sliding to drive changes in cell shape. *Proc. Natl. Acad. Sci. USA* *107*, 12151–12156.
- Jordens, I., Fernandez-Borja, M., Marsman, M., Dusseljee, S., Janssen, L., Calafat, J., Janssen, H., Wubbolts, R., and Neefjes, J. (2001). The Rab7 effector protein RILP controls lysosomal transport by inducing the recruitment of dynein-dynactin motors. *Curr. Biol.* *11*, 1680–1685.
- Kashina, A., and Rodionov, V. (2005). Intracellular organelle transport: few motors, many signals. *Trends Cell Biol.* *15*, 396–398.
- Kim, H., Ling, S.C., Rogers, G.C., Kural, C., Selvin, P.R., Rogers, S.L., and Gelfand, V.I. (2007). Microtubule binding by dynactin is required for microtubule organization but not cargo transport. *J. Cell Biol.* *176*, 641–651.
- Kural, C., Kim, H., Syed, S., Goshima, G., Gelfand, V.I., and Selvin, P.R. (2005). Kinesin and dynein move a peroxisome in vivo: a tug-of-war or coordinated movement? *Science* *308*, 1469–1472.
- Ling, S.C., Fahrmer, P.S., Greenough, W.T., and Gelfand, V.I. (2004). Transport of *Drosophila* fragile X mental retardation protein-containing ribonucleoprotein granules by kinesin-1 and cytoplasmic dynein. *Proc. Natl. Acad. Sci. USA* *101*, 17428–17433.
- Liu, T., Rohn, J.L., Picone, R., Kunda, P., and Baum, B. (2010). Tao-1 is a negative regulator of microtubule plus-end growth. *J. Cell Sci.* *123*, 2708–2716.
- Lu, W., Fox, P., Lakonishok, M., Davidson, M.W., and Gelfand, V.I. (2013). Initial neurite outgrowth in *Drosophila* neurons is driven by kinesin-powered microtubule sliding. *Curr. Biol.* *23*, 1018–1023.
- Lu, W., Lakonishok, M., and Gelfand, V.I. (2015). Kinesin-1-powered microtubule sliding initiates axonal regeneration in *Drosophila* cultured neurons. *Mol. Biol. Cell* *26*, 1296–1307.
- Michel, R., Steinmeyer, R., Falk, M., and Harms, G.S. (2007). A new detection algorithm for image analysis of single, fluorescence-labeled proteins in living cells. *Microsc. Res. Tech.* *70*, 763–770.
- Nakata, T., and Hirokawa, N. (1995). Point mutation of adenosine triphosphate-binding motif generated rigor kinesin that selectively blocks anterograde lysosome membrane transport. *J. Cell Biol.* *131*, 1039–1053.
- Nascimento, A.A., Roland, J.T., and Gelfand, V.I. (2003). Pigment cells: a model for the study of organelle transport. *Annu. Rev. Cell Dev. Biol.* *19*, 469–491.
- Otsu, N. (1979). A threshold selection method from Gray-level histograms. *IEEE Trans. Syst. Man Cybern.* *9*, 62–66.
- Pan, X., Ou, G., Civelekoglu-Scholey, G., Blacque, O.E., Endres, N.F., Tao, L., Mogilner, A., Leroux, M.R., Vale, R.D., and Scholey, J.M. (2006). Mechanism of transport of IFT particles in *C. elegans* cilia by the concerted action of kinesin-II and OSM-3 motors. *J. Cell Biol.* *174*, 1035–1045.
- Pilling, A.D., Horiuchi, D., Lively, C.M., and Saxton, W.M. (2006). Kinesin-1 and Dynein are the primary motors for fast transport of mitochondria in *Drosophila* motor axons. *Mol. Biol. Cell* *17*, 2057–2068.
- Rasband, W.S. (1997–2011). ImageJ. <http://imagej.nih.gov/ij/>.
- Sato, Y., Nakajima, S., Shiraga, N., Atsumi, H., Yoshida, S., Koller, T., Gerig, G., and Kikinis, R. (1998). Three-dimensional multi-scale line filter for segmentation and visualization of curvilinear structures in medical images. *Med. Image Anal.* *2*, 143–168.
- Schroeder, H.W., 3rd, Mitchell, C., Shuman, H., Holzbaur, E.L., and Goldman, Y.E. (2010). Motor number controls cargo switching at actin-microtubule intersections in vitro. *Curr. Biol.* *20*, 687–696.
- Sharp, D.J., Mennella, V., and Buster, D.W. (2005). KLP10A and KLP59C: the dynamic duo of microtubule depolymerization. *Cell Cycle* *4*, 1482–1485.
- Simpson, P.A., and Spudich, J.A. (1980). ATP-driven steady-state exchange of monomeric and filamentous actin from *Dictyostelium* discoideum. *Proc. Natl. Acad. Sci. USA* *77*, 4610–4613.
- Slepchenko, B.M., Semenova, I., Zaliapin, I., and Rodionov, V. (2007). Switching of membrane organelles between cytoskeletal transport systems is determined by regulation of the microtubule-based transport. *J. Cell Biol.* *179*, 635–641.
- Vallee, R.B., Tai, C., and Faulkner, N.E. (2001). LIS1: cellular function of a disease-causing gene. *Trends Cell Biol.* *11*, 155–160.
- Wait, E., Winter, M., Bjornsson, C., Kokovay, E., Wang, Y., Goderie, S., Temple, S., and Cohen, A.R. (2014). Visualization and correction of automated segmentation, tracking and lineaging from 5-D stem cell image sequences. *BMC Bioinformatics* *15*, 328.
- Winter, M.R., Fang, C., Banker, G., Roysam, B., and Cohen, A.R. (2012). Axonal transport analysis using Multitemporal Association Tracking. *Int. J. Comput. Biol. Drug Des.* *5*, 35–48.
- Worby, C.A., and Dixon, J.E. (2004). RNA interference in cultured *Drosophila* cells. *Curr. Protoc. Mol. Biol. Chapter* *26*, Unit 26.5.
- Zhang, X.D. (2007). A new method with flexible and balanced control of false negatives and false positives for hit selection in RNA interference high-throughput screening assays. *J. Biomol. Screen.* *12*, 645–655.